Thermal stability and hardness of Mg-Cu-Au-Y amorphous alloys

Journal of Alloys and Compounds 434–435 (2007) 183–186

Thermal stability and hardness of Mg–Cu–Au–Y amorphous alloys

M. Baricco [a,*], A. Castellero [b], M. Di Chio [a], Zs. Kovacs [c], P. Rizzi [a], M. Satta [a], A. Ziggiotti [a]

[a] Dipartimento di Chimica IFM and NIS, Universit`a di Torino, Via P. Giuria 9, 10125 Torino, Italy
[b] Laboratory of Metal Physics and Technology, ETH Zurich, Wolfgang-Pauli Street 10, CH-8093 Zurich, Switzerland [c]
Department of General Physics, E¨otv¨os Lor`and University, POB 32, H-1518 Budapest, Hungary

Abstract

In this work the effect of Au addition to the GFA of the $Mg_{65}Cu_{25}Y_{10}$ alloy will be discussed. $Mg_{65}Cu_{25}Y_{10}$ and $Mg_{65}Cu_{15}Au_{10}Y_{10}$ amorphous alloys were obtained by rapid solidification. Copper mould casting gave a fully amorphous phase for $Mg_{65}Cu_{25}Y_{10}$, whereas the equilibrium crystalline phases were observed for $Mg_{65}Cu_{15}Au_{10}Y_{10}$. A single eutectic melting reaction was observed for $Mg_{65}Cu_{25}Y_{10}$ but for $Mg_{65}Cu_{15}Au_{10}Y_{10}$ melting is clearly off-eutectic. The presence of an off-eutectic melting of the alloy allows glass formation only by rapid solidification and reduces the glass forming ability. The addition of Au changes the crystallization mechanism of $Mg_{65}Cu_{25}Y_{10}$ amorphous alloy from polymorphic to primary. Two well-separated crystallization peaks were observed for $Mg_{65}Cu_{25}Y_{10}$, whereas for $Mg_{65}Cu_{15}Au_{10}Y_{10}$ the crystallization is more complicated and two overlapped crystallization signals were obtained, followed by a broad exothermal peak at higher temperature. Y-containing Mg_2Cu nanocrystals are formed as first crystallization product for both alloys. The Au-containing sample produces also a nanocrystalline $AuCu_3$ phase. From the indentation tests, a significant increase of hardness was observed in the Au-containing amorphous alloy during crystallization, because of the formation of nanocrystalline phases.

1. Introduction

Mg-based metallic glasses have a general composition $Mg_a(Cu,Ni)_bTM_c(Y,RE)_d$, where TM represents a transition metal and RE is a rare earth ($60 < a < 70$). The simplest binary Mg–Cu and Mg–Ni (c, $d = 0$) systems form metallic glasses only by rapid solidification in a narrow composition range around the eutectic between Mg and Mg_2Cu or Mg_2Ni [1]. The addition of Y or RE ($d = 10$) significantly improve the glass forming abil-ity (GFA) so that bulk metallic glasses (BMG) can be prepared by copper mould casting [2]. Glass formation may be further improved by addition of TM like Ag [3] and Zn [4] ($c = 10$) or by a substitution of Y with a RE [5]. A maximum diameter of 14 mm has been recently reported for a $Mg_{65}Cu_{7.5}Ni_{7.5}Zn_5Ag_5Y_5Gd_5$ BMG prepared in air [6]. Several parameters have been sug-gested to explain the enhancement of GFA by TM addition in Mg-based alloys, but more experimental work is necessary for a complete understanding.

Mg-based metallic glasses show superior mechanical and wear properties and enhanced corrosion resistance with respect to conventional light alloys [7]. Mg-based BMGs are characterized by a brittle fracture [8] but an enhancement of plasticity may be obtained by particle dispersion [9]. The precipitation of nanocrystals by partial crystallization may further improve mechanical properties of monolithic BMG [10].

Au–Pb–Sb alloys show an high GFA, so that amorphous millimeter sized droplets can be obtained by drop tube processing [11]. An amorphous $Au_{80}Cu_{10}Y_{10}$ alloy has been obtained by rapid solidification, showing a crystallization temperature of 685 K, which indicates long-term stability at room temperature for potential applications [12]. So, investigations on the effect of Au-addition on thermal stability and mechanical properties of Mg-based amorphous alloys may contribute to the under-standing of the role of TM on GFA and may extend possible applications for precious metallic glasses.

In this work the effect of Au addition on the GFA and the crystallization mechanism of the $Mg_{65}Cu_{25}Y_{10}$ alloy will be discussed.

2. Experimental

Master alloys were prepared from pure elements by induction melting. Ribbons were prepared by melt spinning. Small ingots (up to 3 mm in diameter) were obtained by injection casting technique into a conical Cu mould. The structure

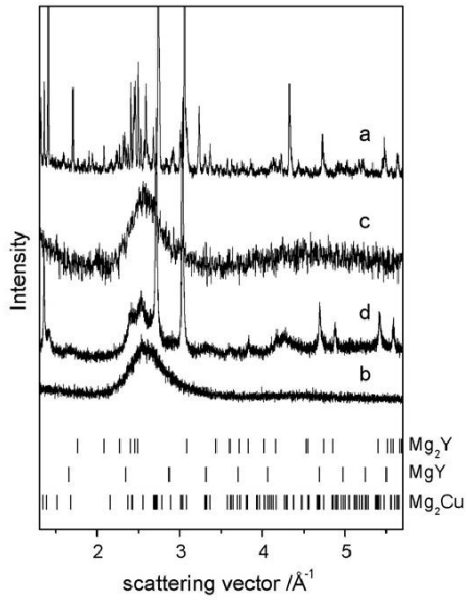

Fig. 1. X-ray diffraction patterns for $Mg_{65}Cu_{25}Y_{10}$ alloys: (a) master alloy; (b) as-quenched ribbon; (c) as-cast ingot with 3 mm diameter; (d) ribbon annealed up to 543 K in the DSC. Intensity data are reported as a function of scattering vector $s = 4\pi \sin\theta/\lambda$, where θ is the diffraction angle and λ is the X-ray wavelength.

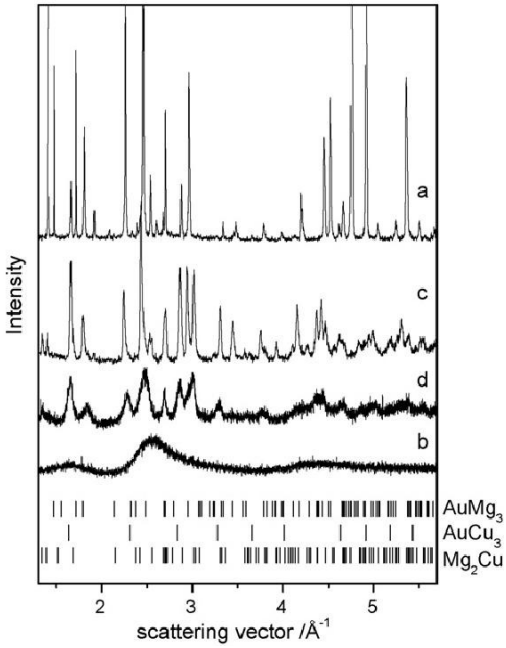

Fig. 2. X-ray diffraction patterns for $Mg_{65}Cu_{15}Au_{10}Y_{10}$ alloys: (a) master alloy; (b) as-quenched ribbon; (c) as-cast ingot with 3 mm diameter; (d) ribbon annealed up to 593 K in the DSC. Intensity data are reported as a function of scattering vector $s = 4\pi \sin\theta/\lambda$, where θ is the diffraction angle and λ is the X-ray wavelength.

and microstructure of various samples were analysed by X-ray diffraction (XRD) and by a microprobe equipped scanning electron microscopy (SEM/EDS). Thermal stability and thermochemical properties were investigated by differential scanning calorimetry (DSC). Indentation tests were carried out, using a stan-dard Vickers microhardness test, to estimate the mechanical properties.

3. Results and discussion

The XRD patterns of $Mg_{65}Cu_{25}Y_{10}$ and $Mg_{65}Cu_{15}Au_{10}Y_{10}$ (at.%) master alloys are reported in curves a of Figs. 1 and 2, respectively. The ternary alloy shows the presence of Mg_2Cu and Mg_2Y phases, together with minor contributions from MgY and unidentified phases. With the addition of Au, Mg_2Cu remains as equilibrium phase, together with $AuCu_3$ and $AuMg_3$, but no Y-containing phases were observed, suggesting a possible dissolution of this element into equilibrium compounds. Rapid solidification produced easily an amorphous phase for both sys-tems, as evidenced by patterns b in Figs. 1 and 2. The asymmetry observed in the amorphous halo of the Au-containing alloy seems to suggest the presence of a nanocrystalline phase embed-ded in the as-quenched amorphous matrix. The reduced GFA due to the Au-addition to the ternary alloy is confirmed by the cop-per mould casting experiments. The results of the XRD analysis of as-cast alloys, reported in patterns c of Figs. 1 and 2, show that a fully amorphous phase was obtained for $Mg_{65}Cu_{25}Y_{10}$, whereas the equilibrium crystalline phases were observed for $Mg_{65}Cu_{15}Au_{10}Y_{10}$. For the latter, a significant refinement of the microstructure was produced by copper mould casting, as evidenced by the line broadening of diffraction peaks.

The DSC analysis for crystallization of amorphous ribbons and the melting of the master alloys, obtained at 0.33 K s^{-1}, are reported in Fig. 3. Two well-separated crystallization peaks were observed for $Mg_{65}Cu_{25}Y_{10}$, followed by a single eutectic melting reaction (curves a). For $Mg_{65}Cu_{15}Au_{10}Y_{10}$ (curves b) the crystallization is more complicated and two overlapped signals were obtained, followed by a broad exothermal peak at higher temperature. Melting is clearly off-eutectic, as evi-denced by a double endothermic peak. T_g is clearly observed at 439 K for the ternary alloy, whereas it is less evident for the Au-containing amorphous alloy and it can be easily evidenced only at higher heating rates. A summary of the results obtained from the DSC analysis is reported in Table 1. The first step of crystallization in $Mg_{65}Cu_{25}Y_{10}$ alloy leads to the formation of a Mg_2Cu phase which showed some textures, probably because

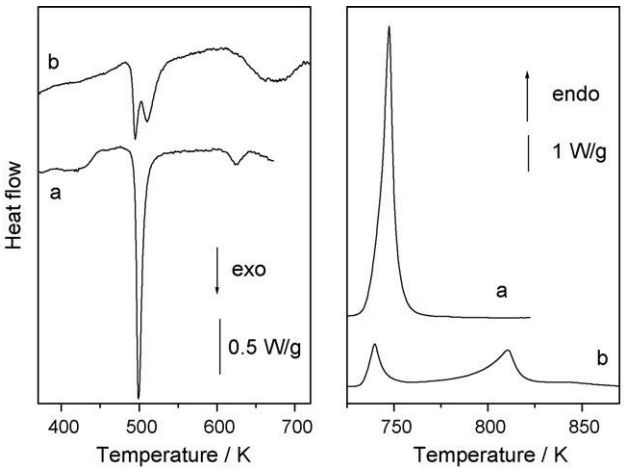

Fig. 3. DSC traces for crystallization of amorphous alloys (left) and melting of master alloys (right) for (a) $Mg_{65}Cu_{25}Y_{10}$ and (b) $Mg_{65}Cu_{15}Au_{10}Y_{10}$. The heating rate was 0.333 K s^{-1}.

Table 1

Results of the DSC analysis for $Mg_{65}Cu_{25}Y_{10}$ and $Mg_{65}Cu_{15}Au_{10}Y_{10}$ amorphous alloys obtained at 0.33 K s^{-1}

Alloy	T_g (K)	T_x (K)	$\_H_x$ (kJ mol^{-1})	E_{att}^1 (kJ mol^{-1})	E_{att}^2 (kJ mol^{-1})	T_m (K)	$\_H_m$ (kJ mol^{-1})
$Mg_{65}Cu_{25}Y_{10}$	439	492	3.6	150	–	734	8.5
$Mg_{65}Cu_{15}Au_{10}Y_{10}$	–	489	2.5	200	210	733	4.5

T_g, glass transition temperature; T_x, onset crystallization temperature; $\_H_x$, enthalpy of first crystallization step; E_{att}^1, activation energy for crystallization (first peak); E_{att}^2, activation energy for crystallization (second peak); T_m, onset melting temperature; $\_H_m$, enthalpy of melting.

of surface crystallization, as evidenced in the XRD pattern of an amorphous ribbon annealed up to 543 K in the DSC (Fig. 1, curve d). An annealing of a $Mg_{65}Cu_{15}Au_{10}Y_{10}$ amorphous ribbon up to 593 K in the DSC (i.e. after the double crystallization peak) leads to the formation of nanostructured Y-containing Mg_2Cu and $AuCu_3$ phases, as evidenced by the significant broadening of diffraction peaks shown in Fig. 2, curve d. The broad exother-mic peak observed in the DSC trace at higher temperatures is likely related to a microstructure coarsening and to precipitation of equilibrium $AuMg_3$ phase.

SEM analysis of $Mg_{65}Cu_{25}Y_{10}$ master alloy showed an eutectic microstructure, confirming the melting behaviour reported in Fig. 3, curve a. No ternary crystalline phases have been reported in structural and thermodynamic databases for the Mg–Cu–Y system, so an equilibrium between binary phases has to be considered. Mg_2Cu is the crystal phase with the higher driving force for nucleation from the liquid phase [13]. In fact it remains as residual phase in as-quenched partially amor-phous samples and it is the first observed crystallization product (Fig. 1, curve d). A second equilibrium phase is Mg_2Y, which has been found as first nucleating phase during isothermal crys-tallization at 433 K [14]. Binary Cu–Y compounds (Cu_2Y and Cu_3Y) have been also reported as equilibrium phases [14,15], but they were not observed in the master alloy. In order to describe the crystallization of $Mg_{65}Cu_{25}Y_{10}$ amorphous alloy, a composition–enthalpy plot is reported in Fig. 4, considering

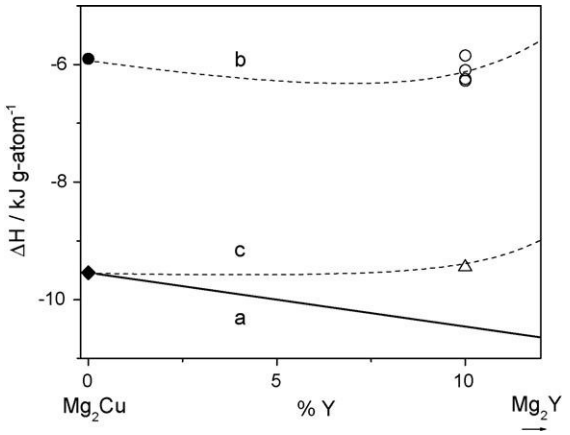

Fig. 4. Composition–enthalpy plot for the Mg_2Cu–Mg_2Y section of the Mg–Cu–Y system. Reference states are hcp-Mg, fcc-Cu and hcp-Y. Curve a, equilibrium compounds; curve b, amorphous phase; curve c, Y-containing Mg_2Y. Open circles: total enthalpy of crystallization for $Mg_{65}Cu_{25}Y_{10}$ (Refs. [4,17,18] and this work). Open triangle: partial enthalpy of crystallization for $Mg_{65}Cu_{25}Y_{10}$ (this work). Full diamond: enthalpy of formation for Mg_2Cu (Ref. [13]). Full circle: enthalpy of amorphous Mg_2Cu (Ref. [16]).

the Mg_2Cu–Mg_2Y section of the ternary system. Enthalpy of equilibrium phases (curve a) have been obtained from the Cal-phad assessment of binary systems [13], whereas the enthalpy of amorphous Mg_2Cu, which is not available experimentally, was taken from molecular dynamic simulations [16]. In order to esti-mate the enthalpy of the amorphous ternary alloys, experimental data for the heat of crystallization of $Mg_{65}Cu_{25}Y_{10}$ amorphous alloy [17,18] have been added to the enthalpy of the crystals mix-ture (curve b). Considering that the first stage of crystallization corresponds to a polymorphous crystallization of the amorphous alloy into a Y-containing Mg_2Cu phase, as already reported in Refs. [17,19], a trend for the enthalpy of Y-dissolution in Mg_2Cu can be estimated (curve c) form the experimental values for the heat released during the first (–3.6 kJ mol^{-1}) and second (–0.4 kJ mol^{-1}) step of crystallization. It is clear that a polymor-phic crystallization of $Mg_{65}Cu_{25}Y_{10}$ amorphous alloy into Y-containing Mg_2Cu may be kinetically favoured. In this case, no solute redistribution is necessary during crystallization and the composition of the residual amorphous matrix remains nearly constant. The crystallization of $Mg_{65}Cu_{15}Au_{10}Y_{10}$ amorphous alloy is more complicated and involves a significant diffusion of components. In fact, during the first stages of crystallization, the successive formation of Y-containing Mg_2Cu and $AuCu_3$ phases was observed. The different crystallization mechanism observed for $Mg_{65}Cu_{25}Y_{10}$ and $Mg_{65}Cu_{15}Au_{10}Y_{10}$ amorphous alloys is confirmed by the values of the activation energy for crystallization, obtained by the Kissinger method and reported in Table 1. In fact, because of Au-diffusion, $Mg_{65}Cu_{15}Au_{10}Y_{10}$ amorphous alloy needs a higher activation energy for crystal-lization with respect to $Mg_{65}Cu_{15}Au_{10}Y_{10}$.

Vickers hardness was measured on as-quenched and annealed $Mg_{65}Cu_{25}Y_{10}$ BMG and $Mg_{65}Cu_{15}Au_{10}Y_{10}$ amorphous ribbon. The results are reported in Fig. 5 as a function of transformed fraction, as deduced from a progressive integration of the DSC crystallization peaks shown in Fig. 3. From the indentation tests, an initial increase in hardness was observed for both alloys as a consequence of crystallization. $Mg_{65}Cu_{25}Y_{10}$ BMG shows a maximum hardness of about 370 HV at the early stages of crys-tallization, reaching a final value of about 320 HV at the end of the transformation. On the contrary, $Mg_{65}Cu_{15}Au_{10}Y_{10}$ displays a progressive increasing of the hardness, up to a final value of about 430 HV for a fully crystalline sample. Both a maximum and a progressive increase of hardness as a function of trans-formed fraction has been observed in Mg-based BMGs [10,20]. The effect of a crystalline phase embedded in the amorphous matrix on hardness is strongly related to the size of crystal par-ticles and to the composition of the residual amorphous matrix [21].

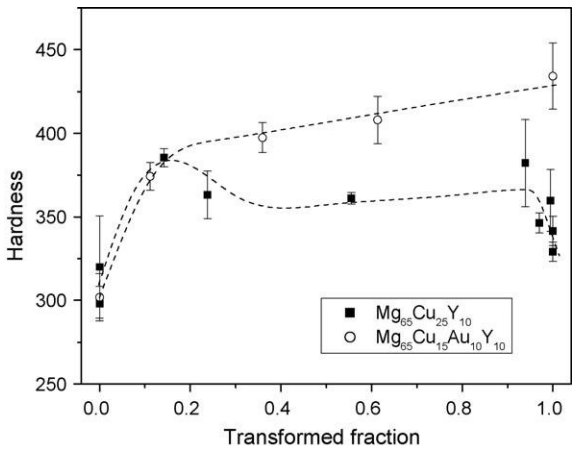

Fig. 5. Hardness of $Mg_{65}Cu_{25}Y_{10}$ and $Mg_{65}Cu_{15}Au_{10}Y_{10}$ amorphous alloys as a function of transformed fraction calculated from integration of first DSC crystallization peak.

In fact, nanosized particles dispersed in the amorphous matrix may interact with shear bands during the deformation, acting either as barrier for propagation and as sites for their nucleation, leading to a microstructure which improve mechanical proper-ties during crystallization, as obtained for $Mg_{65}Cu_{15}Au_{10}Y_{10}$ amorphous alloy. On the other hand, the presence of precipi-tates bigger than a typical size for shear bands in amorphous alloys (about 30 nm) has a little effect on plastic deformation of the amorphous matrix and the hardness of the composite can be related to the volume fraction of intermetallic phases [10], as observed in $Mg_{65}Cu_{25}Y_{10}$.

4. Conclusions

The effect of Au addition to $Mg_{65}Cu_{25}Y_{10}$ alloy on glass formation was discussed.

Rapid solidification gives an amorphous alloy for both $Mg_{65}Cu_{25}Y_{10}$ and $Mg_{65}Cu_{15}Au_{10}Y_{10}$ alloys, but copper mould casting gave a fully amorphous phase only for $Mg_{65}Cu_{25}Y_{10}$, whereas the equilibrium crystalline phases were observed for $Mg_{65}Cu_{15}Au_{10}Y_{10}$. A single eutectic melting reaction was observed for $Mg_{65}Cu_{25}Y_{10}$ but for $Mg_{65}Cu_{15}Au_{10}Y_{10}$ melting is clearly off-eutectic, so that the glass forming ability appears strongly reduced. The addition of Au changes the crystallization mechanism of $Mg_{65}Cu_{25}Y_{10}$ amorphous alloy from polymorphic to primary. For both alloys, Y-containing Mg_2Cu nanocrystals are formed as first crystallization product.

Because of the formation of nanocrystalline phases, a signif-icant increase of hardness was observed in the Au-containing amorphous alloy during crystallization.

Acknowledgments

Work performed for COFIN/MIUR 2002030504 004 and for MRTN-CT-2003-504692.

References

[1] A.T.W. Kempen, H. Nitsche, F. Sommer, E.J. Mittemejer, Metall. Mater. Trans. 33A (2002) 1041.
[2] N.H. Pryds, Mater. Sci. Eng. A 375–377 (2004) 186.
[3] E.S. Park, H.G. Kang, W.T. Kim, J. Non-cryst. Solids 279 (2001) 154.
[4] H. Men, Z.Q. Hu, J. Xu, Scritpa Mater. 46 (2002) 699.
[5] H. Men, D.H. Kim, J. Mater. Res. 18 (2003) 1502.
[6] E.S. Park, D.H. Kim, J. Mater. Res. 20 (2005) 1465.
[7] G. Yuan, C. Qin, A. Inoue, J. Mater. Res. 20 (2005) 394.
[8] X.K. Xi, D.Q. Zhao, M.X. Pan, W.H. Wang, Y. Wu, J.J. Leeandowski, Phys. Rev. Lett. 94 (2005) 125510.
[9] Y. Xu, H. Ma, J. Xu, E. Ma, Acta Mater. 53 (2005) 1857.
[10] U. Wolff, N. Pryds, E. Johnson, J.A. Wert, Acta Mater. 52 (2004) 1989.
[11] M.C. Lee, J.M. Kendall, W.L. Johnson, J. Appl. Phys. Lett. 40 (1982) 382.
[12] B.C. Giessen, S.V. Gokhale, K.G. Marchev, US Patent 005593514A (1994).
[13] D. Kim, B. Lee, N.J. Kim, Scripta Mater. 52 (2005) 969.
[14] H. Men, W.T. Kim, D.H. Kim, J. Non-cryst. Solids 337 (2004) 29.
[15] A. Inoue, A. Kato, T. Zhang, S.G. Kim, T. Masumoto, Mater. Trans. JIM 32 (1991) 609.
[16] N.P. Bailey, J. Schiøtz, K.W. Jacobsen, Phys. Rev. B 69 (2004) 144205.
[17] B.S. Murty, K. Hono, Mater. Trans. JIM 41 (2000) 1538.
[18] A. Inoue, T. Nakamura, N. Nishiyama, T. Masumoto, Mater. Trans. JIM 33 (1992) 937.
[19] J. Zhang, H.F. Zhang, M.X. Quan, Z.Q. Hu, Scripta Mater. 49 (2003) 485.
[20] Zs. Kovacs,´ A. Castellero, A.L. Greer, J. Lendvai, M. Baricco, Mater. Sci. Eng. A 387–389 (2004) 1012.
[21] A.L. Greer, Mater. Sci. Eng. A 304–306 (2001) 68.